ORIGINAL ARTICLE

In silico prediction coupled with in vitro experiments and absorption modeling to study the inclusion complex of telmisartan with modified beta-cyclodextrin

Abhishek Chandra[1] · M. Vivek Ghate[1] · K. S. Aithal[2] · Shaila A. Lewis[1]

Abstract
Telmisartan (TEL) is a poorly bioavailable antihypertensive drug candidate owing to its low solubility in all the biofluids. The present study is aimed to enhance the solubility of TEL by forming an inclusion complex with sulfobutylether beta-cyclodextrin (SBE-β-CD), discover its mode of inclusion and predict the bioavailability of the prepared complexes. The formation of the inclusion complex is explained based on the hydrogen bond propensities and molecular dynamics simulations. Freeze-drying method was employed for the preparation of inclusion complexes. These complexes were subsequently characterized by powder X-ray diffraction, differential scanning calorimetry, and Fourier transform-infrared spectroscopy. The spatial configuration of the drug inside the cyclodextrin cavity is probed using ^{1}H and ^{13}C NMR. The in silico docking results are in good agreement with the experimental data and reveal that the hydrogen bond is formed as a part of the guest molecule enters from the broader end of the ring and the protons at the interior portion of the molecule interact with the carboxylic acid (–COOH) group of TEL leading to the formation of a hydrogen bond. The phenyl moiety of TEL occupies the central core and forms multiple Van-der-Waals interactions with the glucopyranose units of the SBE-β-CD. The inclusion complex demonstrates significantly higher in vitro dissolution profile as compared with plain TEL. The GastroPlus™ simulation software generated parameters of inclusion complex in comparison to plain TEL show a seven fold increase in C_{max} and 18 fold increase in bioavailability.

Keywords Telmisartan · Sulfobutylether beta-cyclodextrin · Solubility enhancement · Inclusion complexes · Molecular modeling · GastroPlus™

Introduction

Oral pathway, though the preferred route for administering antihypertensives, poses many challenges to the formulator. Ensuring adequate bioavailability from an oral formulation is a key concern as it is dictated by factors such as solubility, stability as well as absorption. Telmisartan (TEL) an angiotensin II receptor blocker is a widely prescribed antihypertensive owing to its potent, long-acting nature, selective mechanism of action and considerable safety of use [1]. Moreover, recent literature reports potential of TEL in prevention and treatment of human cancers as well [2, 3]. TEL interferes with the binding of angiotensin II to the angiotensin II AT1-receptor by binding reversibly and selectively to the receptors in vascular smooth muscle and the adrenal gland. After oral administration part of a dose is conjugated with glucoronate in intestine and accumulated in the liver. No pharmacological activity has been shown for the conjugate. TEL elimination is characterised by biexponential decay pharmacokinetics with a terminal eliminate ion half-life of > 20 h [4, 5].

Although TEL is superior regarding activity it has poor oral bioavailability due to low solubility (BCS class II) [6–8]. Hence, it would be desirable to offer a formulation that could avoid administration of the unreasonably large amounts of the TEL, while at the same time provide the desired increase in the rate of therapeutic onset.

✉ Shaila A. Lewis
   s.lewis@manipal.edu

1   Department of Pharmaceutics, Manipal College
    of Pharmaceutical Sciences, Manipal Academy of Higher
    Education, Manipal 576104, India

2   International Center for Applied Sciences, Manipal Academy
    of Higher Education, Manipal 576104, India

Therefore, improving solubility is of paramount importance. Various techniques are used for the enhancement of the solubility of poorly soluble drugs which include particle size reduction, crystal engineering, salt formation, solid dispersion, use of surfactant, complexation, nanosuspension and cryogenic techniques. Selection of solubility improving method depends on drug property, site of absorption, and required dosage form characteristics [9, 10].

Among the formulation techniques explored for solubility enhancement, cyclodextrins (CDs) have emerged as a significant tool. CDs can enhance apparent water solubility by establishing dynamic, non-covalent, water-soluble inclusion complexes [11]. Although the natural cyclodextrin (β-CD) is hydrophilic, it has limited solubility and is reported to exhibit nephrotoxicity [12, 13].

Sulfobutylether beta-cyclodextrin (SBE-β-CD), a hydrophilic derivative of β-CD, has substitute groups in a favorable location for entry of guest into the CD cavity thereby enhancing complexation efficiency. Besides these attributes the charge of the CD molecule is positioned at a site as far as possible from the hydrophobic cavity, thus increasing its solubilizing capacity [14].

The present research work explores the enhancement of solubility of TEL by inclusion with SBE-β-CD (Fig. 1). Various physical characterization techniques were used to characterize the TEL–SBE-β-CD complex. The modeling of the resulting complex was done in silico by molecular mechanics, and molecular dynamics was used to interpret the binding positions and to estimate the relative binding affinities. Furthermore, dissolution profiles obtained in relevant medium combined with absorption modeling using GastroPlus™ software was employed to quantitatively predict human pharmacokinetics of the developed inclusion complexes of TEL.

Experimental

Materials

Telmisartan (TEL), molecular weight 514 Da, was a gift sample from Cadila Pharmaceuticals, India. Sulfobutylether beta-cyclodextrin (average molecular weight: 2163 g mol^{-1}) was kindly provided by CyDex Pharmaceuticals, USA. All other reagents used in the study were of analytical grade and used as obtained.

In silico molecular modeling studies

Molecular modeling studies of TEL inclusion complexes

The molecular modeling studies of TEL with SBE-β-CD was carried out using the Mercury (Version 3.8) and GOLD (Version 5.4.1) software's available under the Cambridge Structural Database (CSD) suites, UK. Processing of the docked structures and molecular dynamics (MD) were carried out in the Chem3D software (Version 15.1) available under the ChemOffice 2015 suite, PerkinElmer, UK.

Structure collection

The crystal structure of TEL was obtained from the CSD represented by the Cambridge Crystallographic Data Centre (CCDC) identification number 209544 [15]. The obtained crystal structure was energy minimized using the modified Allinger's MM2 force field in Chem3D [16]. The crystal structure of β-CD was extracted from the protein structure 1BFN obtained from the protein data bank (PDB). The structure of the protein was processed initially using GOLD software, and then β-CD was extracted and used for the simulation study. SBE-β-CD was generated by attaching sulfobutyl group on the 6-OH group of glucopyranose manually to the β-CD in the Chem3D software. The generated SBE-β-CD
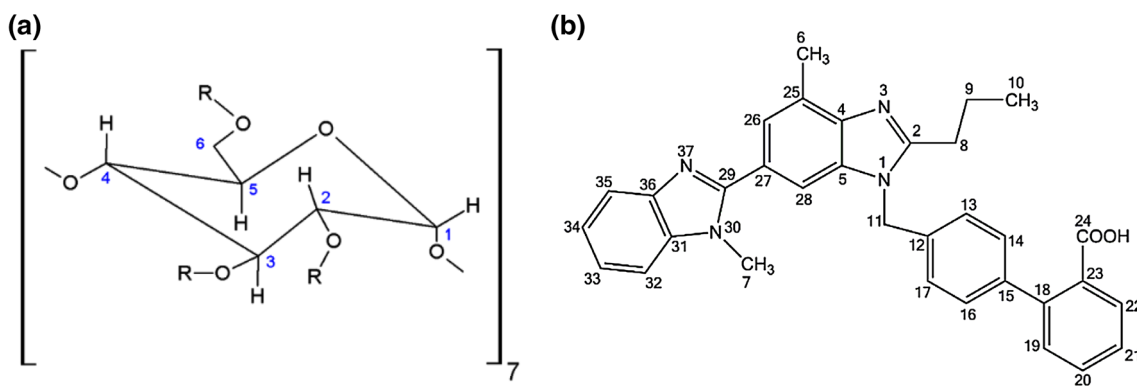

Fig. 1 Structure of **a** SBE-β-CD (R=H) or (CH$_2$)$_4$SO$_3$ and **b** structure and numbering of TEL

structure was energy minimized to a minimum RMS gradient of 0.010 [17].

Hydrogen bonding patterns for TEL

Hydrogen bonding patterns for TEL was studied using the hydrogen bond propensities calculations in the Materials module available in the Mercury software [18, 19]. The estimates take into account the statistical model built from structures that are available in the CSD and predicts the probabilities for hydrogen bond pairings to form a linkage with the molecule of interest.

Generation of supramolecular inclusion complex models

Molecular docking was carried out for generating SBE-β-CD inclusion complexes using the GOLD software. Initially, the cavity was produced by selecting all atoms within a radius of 10 Å utilizing the docking Wizard. TEL was docked to SBE-β-CD and scored with GoldScore and rescored with ChemScore to generate supramolecular inclusion complex.

Fitness functions

GoldScore and ChemScore

The GoldScore embedded by default in the GOLD was used to primarily predict the guest-binding positions during the formation of inclusion complexes [20]. GoldScore takes into account the hydrogen-bond energy, van der Waals energy, and torsion strain. On the other hand, the docking process was rescored using the ChemScore option which included the term 'ΔG' representing the total free energy change that takes place on successful formation of the inclusion complexes. ChemScore also within itself incorporates the hydrogen bonding, ligand flexibility, and hydrophobic contact area.

GoldScore uses the bond strengths in the form of:

$$GoldScore = X_{hb\_ext} + X_{vdw\_ext} + X_{hb\_int} + X_{vdw\_int} \quad (1)$$

where X_{hb_ext} is the host–guest hydrogen bonding score, X_{hb_int} is the internal hydrogen bonding of the guest molecule and, X_{vdw_ext} and X_{vdw_int} are the scores that usually arise from the weak Van der Waals forces.

ChemScore is trained by regression and measures the total free energy as:

$$\Delta G_{binding} = \Delta G_0 + \Delta G_{Ghbond} + \Delta G_{metal} + \Delta G_{rot} + \Delta G_{lipo} \quad (2)$$

where ΔG_0 is the regression coefficient, and remaining terms are obtained by the multiplication product of respective regression coefficients and the physical contributions from hydrogen bonds, metal binding, lipophilic groups and rotational torsions.

Molecular dynamics simulation

Chem3D was used for running MD simulations using the MM2 method based on Newton's equations of motion to simulate the movements of atoms. TEL–SBE-β-CD inclusion complex was loaded onto the visualizer, and the molecular dynamics computation was carried out consisting of a series of steps occurring at an interval of 2.0 fs and a frame interval of 10 fs. The simulations were set to terminate after 10,000 steps. New positions and velocities of each of the atoms were calculated by the Beeman algorithm. The dynamics computation in Chem3D also allows for the adjustments to be made according to the temperature, hence in the study the calculations were carried out at a heating and cooling rate of 1.0 kcal atom^{-1} ps^{-1} with a target of 300 K. The visualization box containing TEL–SBE-β-CD inclusion complex with solvent was minimized and MD simulation at set conditions. Saving energy and structure enumerated for every iteration of increase in the number of steps during simulation generated the trajectory. The final stable structure was analyzed for the energies, steps and plotted as the RMSD curve.

Phase solubility of TEL

Phase-solubility of TEL in SBE-β-CD solutions were determined according to the procedure first reported by Higuchi and Connors [21]. Briefly, to an excess of TEL was dispersed in an aqueous solution of varying concentrations of SBE-β-CD (25 ml). The resulting dispersions were then vortexed and constantly agitated on a rotary shaker at a constant temperature range of 37 ± 2 °C for 24 h. After filtration (0.45 μm) the samples were suitably diluted, and the concentration of TEL was determined by HPLC (Shimadzu LC-2010CHT, Koyoto Japan). Solubility studies were performed in triplicate. A graph was then plotted with millimoles of TEL against millimoles of SBE-β-CD. The apparent binding was expressed as the stability constant (K_c) given by the formula:

$$K_c = \frac{Slope}{X_0}(1 - Slope) \quad (3)$$

where K_c is the apparent binding/ stability constant and X_0 is the solubility of the TEL in the absence of SBE-β-CD.

Preparation of inclusion complex of TEL with SBE-β-CD

Freeze drying method

Equimolar ratios of TEL and SBE-β-CD (1:1) were dissolved in 0.1 N NaOH solution separately until a clear homogeneous solution of was obtained. These solutions were stirred for 1 h and frozen at − 80 °C for 4 h and freeze-dried for 48 h at − 45 °C under vacuum in a freeze drier (Labtech, Daihan Labtech India Pvt. Ltd, India). The product was stored in a desiccator after sieving until use [22].

Physicochemical characterization of TEL–SBE-β-CD

Differential scanning calorimetry (DSC)

The DSC thermograms were recorded on a DSC (DSC-50, Shimadzu, Japan) of the pure TEL, SBE-β-CD, their physical mixture and the inclusion complex. The samples were weighed into aluminum pans, sealed and heated under nitrogen flow at a scanning rate of 10 °C min^{-1} to obtain a temperature range from 25 to 300 °C. The calibration of the baseline was done using empty aluminum pans as a reference, and temperature/enthalpy using indium.

Fourier transform infrared spectroscopy (FTIR)

The FT-IR spectra (Shimadzu-FTIR 8300) were recorded based on the KBr pellet technique for pure TEL, SBE-β-CD, their physical mixture and the inclusion complex in the wavelength region of 4000–400 cm^{-1}.

X-ray powder diffraction (PXRD)

Rigaku Miniflex 600 X-ray diffractometer (Rigaku Co., Tokyo, Japan) was used to record the PXRD patterns of pure TEL, SBE-β-CD, their physical mixture and the inclusion complex with Cu-kαX-radiation. Instrument was functioned by X-ray tube (600 watts), with a fixed tube current (15 mA) and a voltage (40 kV). A graphite monochromator was used to monochromate the diffracted X-ray beam and the detector used was a standard scintillation counter. X-ray diffraction patterns were recorded over 2θ range of 4°–50° at a scan rate of 4 °C min^{-1}.

Nuclear magnetic resonances (NMR)

The Bruker instrument was used for proton (^{1}H) and carbon (^{13}C) NMR. The pure drug and complex were dissolved in DMSO separately and analyzed. After assigning the signals for various carbon atoms in cyclodextrin and TEL, the changes in chemical shift corresponding to the carbon atom was accounted and recorded.

Dissolution profiles

Media preparation The relevant media to simulate the actual in vivo conditions were prepared according to the method outlined earlier for oral route [23].

Solubility studies

Solubility studies were performed with the pure drug and inclusion complex. Various compendial buffer media were chosen to represent the range of pH values in the upper human gastrointestinal tract (GIT), i.e., stomach and upper small intestine. Biorelevant media were used to better mimic conditions in the upper small intestine. Also, the selection of media took into account media corresponding to BCS requirements (pH 1.2, 4.5 and 6.8) [24]. The set of test media therefore comprised of Simulated Gastric (SGF pH 1.2), the bile salt and lecithin-containing Fed State Simulated Intestinal Fluid (FeSSIF) pH 5.0 and Fasted State Simulated Intestinal Fluid (FaSSIF) pH 6.5 and acetate buffer pH 4.5 [23, 25].

In vitro dissolution

USP type 1 apparatus was used to carry out the dissolution at a stirring rate of 50 rpm. Dissolution media (900 ml) was maintained at 37 ± 0.5 °C to mimic the in vivo conditions. At appropriate time interval samples were collected and filtered (0.45 μm) and analyzed using validated HPLC method.

HPLC method

The quantification of TEL was done by RP-HPLC method (Shimadzu, Koyoto, Japan) using Grace Vydac RP C-18 Column (250 × 4.6 mm, 5 μm) column. Methanol:phosphate buffer pH 6.8 (70:30) was used as mobile phase. A constant flow rate of 1 ml min^{-1} was maintained throughout the analysis. The eluent was analysed at 296 nm by a UV detector. The developed method was also validated for accuracy and precision.

In silico determination of the pharmacokinetic parameters

Modeling of the extent of absorption and determination of the pharmacokinetic (PK) parameters of the TEL inclusion complex was carried out in GastroPlus™ (version 9.0, Simulations Plus Inc, Lancaster, CA, USA). The program uses the advanced compartment and absorption transit (ACAT) model to calculate the fraction of the drug absorbed in each

compartment of the intestine. Data input involves the compilation of the compound, physiology and pharmacokinetic tabs. The required input parameters related to TEL physicochemical and pharmacokinetic properties were experimentally determined, in silico predicted and/or taken from the literature. Table 1 represents a summary of the input parameters used in the study.

The pH-solubility profile determined experimentally was employed for all simulations. The effect of bile salt concentration on solubility was also considered using the specific option in the software adjust solubility for salt effect in the dissolution model screen [26]. GastroPlus™ model based on the structure of TEL was employed to estimate the effective human permeability (P_{eff}). TEL absorption model was built considering gut and liver metabolism by UGT enzymes, transporter (OATP1B3) effects in the liver, permeability type tissue as well as entero-hepatic circulation. Based on the previously published literature, the renal clearance was fixed to zero [27]. The reported in vitro kinetic constants Vmax values of 6.7 pmol min^{-1} mg^{-1} protein and K_m of 0.81 μM were converted to in vivo conditions using the Metabolism and Transporter units converter module [28]. Blood/plasma concentration ratio $R_{B/P}$ and unbound percent in plasma (F_{up}, %) were taken from literature [29]. In the physiology module, the ASF opt log D model SA/v6.1 absorption model was selected using the setting human physiology in a fasted state. The software adjusts physiological variables according to selected conditions.

Table 1 Basic modeling input parameters of TEL fed into the GastroPlus™ software

Basic modelling parameters of telmisartan

Parameters	Value
Molecular weight (g mol^{-1})	514.63[a]
Log P	5.8[a]
pKa	4.71[a]
Solubility (mg ml^{-1})	0.081[b]
Human permeability [P_{eff} (cm s^{-1} × 10^4)]	1.11[c]
Mean precipitation time (s)	900[c]
Particle density (gml^{-1})	1.2[c]
Diffusion coefficient (cm^2 s^{-1} × 10^5)	0.54[c]
Clearance$_{bile}$ [CL (l h^{-1})]	0.62[d]
Volume of distribution at steady state [V_{ss} l kg^{-1}]	7[e]
Blood/plasma concentration ratio ($R_{B/P}$)	0.79[e]
Unbound percent in plasma [F_{up} (%)]	0.005[e]

[a]Predicted by ADMET predictor (Version 7.2.0.0, Simulations Plus, Inc., Lancaster, CA, USA)

[b]Experimental value

[c]Default GastroPlus™

[d]Calculated by GastroPlus™

[e]Literature value

The human in vivo data of TEL after intravenous (IV) bolus and oral administration were obtained from the values provided in the literature, digitized and loaded into PK Plus module [28, 30]. The best fit was imported into PK tab to enable software prediction. The built base absorption model was validated using the plasma data comparing the predicted with the observed values.

After building the model for IV human data, the model was extended to oral administration. The predicted PK parameters such as Cmax, Tmax, AUC$_{(0−\infty)}$ were compared with PK parameters reported in the literature. Prediction fold error was taken as a parameter to determine the accuracy of prediction of the PK parameters, and if prediction values were within twofold of observed values, then the simulated model was considered to be of high prediction accuracy [31].

PK simulation for TEL inclusion complex in humans

After successfully building the base model, as an input function into GastroPlus™ and to stimulate the absorption profile, the dissolution data of the inclusion complex in biorelevant media was used. Dissolution and controlled release dispersed (CR-dispersed) data input functions were used to load the respective in vitro dissolution profiles into the software. The software then used the drug release profiles to determine plasma drug concentration.

Results and discussion

Molecular modeling studies of TEL inclusion complexes

Hydrogen bonding patterns of TEL

The crystal packing of TEL showed that the neighboring molecules were held together by hydrogen bonds between the aromatic carboxylic acid and the imidazole ring. Precisely the bonds occurred between HO–C=O and –N=C–N– functional groups of the TEL. A CSD survey was also performed with these two functional groups to explain the possible interactions that might take place upon complexation with the SBE-β-CD. The HBP calculator generated a match of 3973 structures for aromatic carboxylic acid and 832 structures for imidazole groups. Taking an equal number of the obtained structures, a logit model was developed for the prediction of HBP comprising of the donor atoms, acceptor atoms, competition, steric densities, and aromaticity.

The hydrogen bond logit model equation was given as follows:

$$HBP = 1/(1 + \exp(−z))$$

where Logit function, z = 3.17966 + 0.345 (donor other) + 2.405 (acceptor atom of imidazole)—2.266 (acceptor atom of aromatic carboxylic acid) + 1.352 (acceptor other)—0.035 (competition)—0.033 (donor steric density)—0.043 (acceptor steric density)—0.386 (donor aromaticity)—0.786 (acceptor aromaticity).

All the model terms were found to be having optimal significance with an area under the receiver-operating characteristics (ROC) curve of 0.8431 indicating excellent discrimination and a goodness-of-fit allowing the model to be viable for the prediction of hydrogen bond formation. The calculations show that the pattern of interaction between the TEL and host molecules is likely to involve the aromatic carboxylic acid or the imidazole ring structures.

Supramolecular inclusion complex models

Energy minimization was carried out for the best-docked pose obtained after docking TEL with SBE-β-CD. As seen in Fig. 2, TEL had a special fit with the host molecule upon inclusion into the hydrophobic cavity. TEL exhibited several intermolecular interactions that were later used to estimate the binding energy as fitness functions. Intermolecular interactions involved the hydrogen bonds, Van der Waals forces, and hydrophobic non-bonded interactions. The carboxyl group from TEL formed multiple hydrogen bonds with the

Fig. 2 Docking binding pose of TEL in the cavity of SBE-β-CD during the formation of the inclusion complex. TEL is shown in blue color, and the SBE-β-CD represented in gray colour. Oxygen atoms are coloured red whereas the sulfur atoms and hydrogen atoms are represented in yellow and white colours respectively. The green coloured dotted line represent the hydrogen bonds; the orange coloured dotted lines represent the other types of interactions like Van Der Waals interactions and hydrophobic bonds. (Color figure online)

hydroxyl group of the glucopyranose of SBE-β-CD. There were multiple glucopyranose subunits involved in the hydrogen bond, with the carboxyl group indicating the presence of strong interaction. A bifurcated hydrogen bond was seen to be formed with the carboxyl group (–C=O moiety) and the hydroxyl group (–OH) attached to the C2 and C3 carbon atoms of the second and third glucopyranose units of SBE-β-CD. It was also noticeable that a hydrogen bond was also formed between the hydroxyl moiety of the carboxyl group and the hydroxyl group attached to the C3 carbon of the seventh glucopyranose unit of SBE-β-CD. The hydrophobic central cavity of the SBE-β-CD was seen to be occupied largely by the second phenyl moiety of TEL majorly linked with multiple Van der Waals interactions between them. Several non-bonded interactions were also observed between the ether-groups of the glucopyranose units and the phenyl rings of TEL. The imidazole moiety of TEL occupied the space in between the sulfobutyl moieties towards the open end of the cyclodextrin, thereby appearing to be hanging from the central core of the SBE-β-CD. The second imidazole moiety formed hydrophobic interactions with sulfobutyl moiety attached to the fourth and fifth glucopyranose ring.

Fitness functions

GoldScore and ChemScore

The 'ΔG' is a measure of binding affinity, calculated considering strain energy terms of ligand and the host. From the MM2 force field, the potential energy of the inclusion complex was calculated. The fitness functions available for docking in the GOLD software were taken as indicative of the favorable binding position and determination of the total energy of the complex. The GoldScore fitness function was 61.451 and ChemScore of 32.588 indicating that out of the ten docked poses given by the software, the best dock-fit was observed for the selected position. Further, based on the terminologies used in the calculation of the fitness functions, the total free energy 'ΔG' was -41.442 kcal mol^{-1}, internal torsion was -8.175 kcal mol^{-1} and hydrogen bond energy was -6.0278 kcal mol^{-1}. The contribution from the lipophilic groups was shown to be equal to -34.584 kcal mol^{-1}. The GoldScore also represented the contribution from the Van der Waals interactions to the extent of -41.682 kcal mol^{-1}. The energy calculation exhibited similar trend where the contribution from Van-der-Waals interaction was higher compared to that of the other electrostatic interactions. It is evident form docking interaction analysis that, the large proportion of the TEL involving one of the phenyl moiety and the imidazole moiety of the molecule was stabilized by hydrophobic interaction within the inclusion complex. The electrostatic interaction was observed with the carboxylate moiety of the TEL. The molecule with
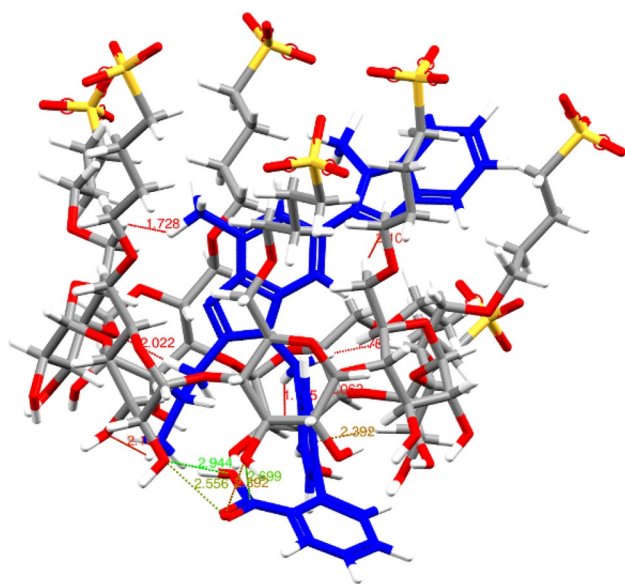
the higher hydrophilic area is easily solubilized in aqueous media. Using the electrostatic mapping tool available in the Mercury, the acceptor–donor molecules of the ligand and the host were visualized. TEL and the inclusion complex had acceptor molecules represented by the red color and donor molecules represented by the cyan color in Fig. 3. The distribution of the group's show that the hydrophilic area, expressed regarding acceptor and donor molecules of TEL was very less compared to the same in the inclusion complex. This was clearly in sync with the experimental results wherein the saturation solubility of the inclusion complex was seen to be higher for the inclusion complex than TEL alone. The docking study predicted a tight-fitting binding of the TEL within the cavity of SBE-β-CD (Fig. 4). The exact location of the hydrogen bond and various Van-der-Walls interaction between the guest and host could be fairly identified from these studies.

Molecular dynamics (MD) simulations

The final docked pose of the inclusion complex had a total energy of 121.074 kJ mol^{-1}. The molecular modeling using MM2 force field also represented the dipole–dipole interaction to be -42.461 kJ mol^{-1} and the Van der Waals interaction to be -154.599 kJ mol^{-1}. The predicted binding pose of TEL with SBE-β-CD by docking study was analyzed by running the MD simulations. All the structural frames enumerated during MD simulation was saved in the output box and analyzed to check the stability of the complex. Based on all the frames enumerated in the trajectory, the root mean square deviation (RMSD) was calculated for SBE-β-CD host and TEL. The RMSD value observed during the simulation indicates the structural stability of predicted inclusion complex; a value within 2.0 Å for RMSD indicates that the complex formed a stable system and is likely to be observed in wet-lab experiments. In the initial phase of MD simulation, as seen in the graph of RMSD versus the iterations the inclusion complex gets stabilized with a drop in the RMSD values. Each iteration represented the increase in the frame steps at an interval of 2.0 fs. After that, the fluctuations in the RMSD values were seen to oscillate between values less than 2.0 Å units. The Fig. 5 shows the RMSD plot of structures evolved in MD simulation to the original structure. The inclusion complex and TEL exhibited RMSD within the range of 0.35 and 0.42 Å indicating the formation of the stable system.

Fig. 3 Hydrophobic and hydrophilic surface area of **a** TEL and **b** TEL-SBE-β-CD inclusion complex. Cyan color represents the hydrophilic area, and red color represents the hydrophobic area. (Color figure online)
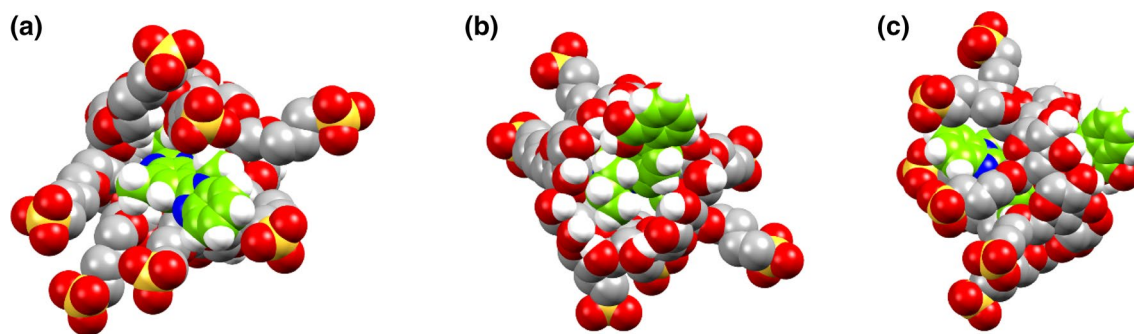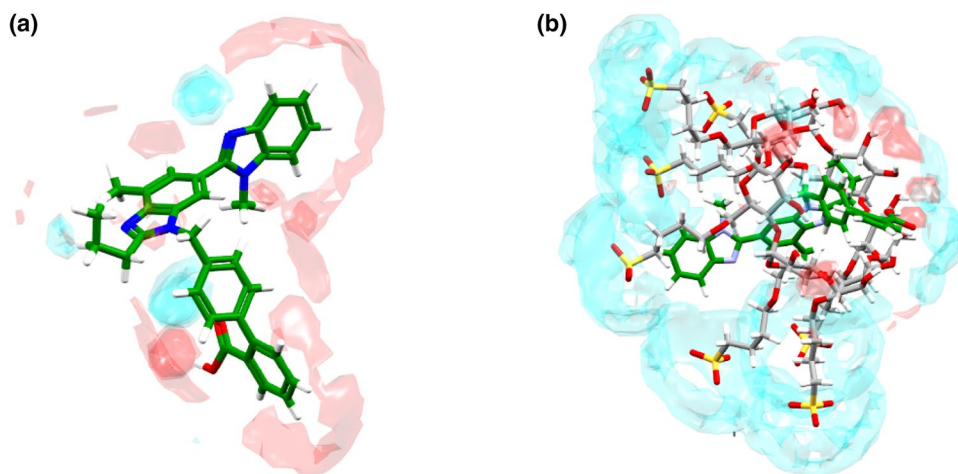

Fig. 4 Tight binding of the TEL with SBE-β-CD. **a** Top view, **b** bottom view and **c** side view. (Color figure online)
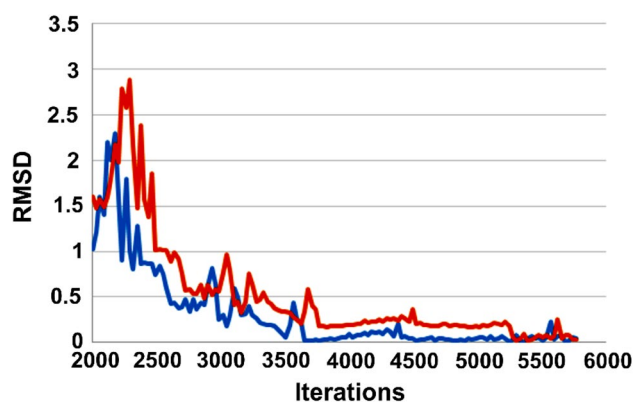
Fig. 5 RMSD plots between the original structure and the structures enumerated during MD simulation. The blue color line indicates the RMSD (Å) fluctuations observed for TEL and the red color line indicates the RMSD fluctuations observed for SBE-β-CD. (Color figure online)

Phase solubility

Based on the Higuchi and Connors model, the shape of the solubility diagram follows an AL—type system (Fig. 6) which indicated a linear trend in the increase of TEL solubility as a parameter dependent on the CD concentration over the complete series of the concentration tested. This suggested the formation of soluble complexes concerning CD concentration. The apparent stability constant [Kc] as calculated by Eq. (1) of TEL:SBE-β-CD complex [1:1] was calculated as 232 M^{-1} from the linear plot.

Differential scanning calorimetry analysis

Following observations were made from the DSC thermal analytical profile of pure TEL, SBE-β-CD, the physical mixtures and inclusion complex (Fig. 7). A sharp melting peak of TEL appears at 273.8 °C ($\Delta H = -103$ J g^{-1}). No dehydration/thermal relaxation peak appears around 100 °C which is due to anhydrous nature of the crystals. SBE-β-CD, on the other hand, showed the dehydration or thermal relaxation
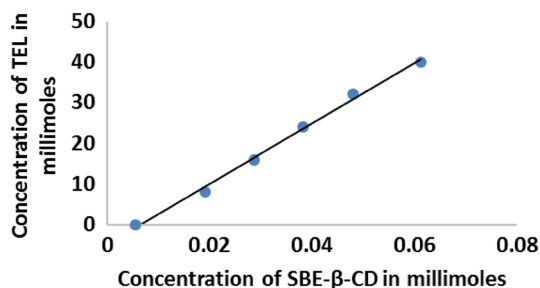

Fig. 6 Phase solubility curve of TEL in different concentrations of SBE-β-CD
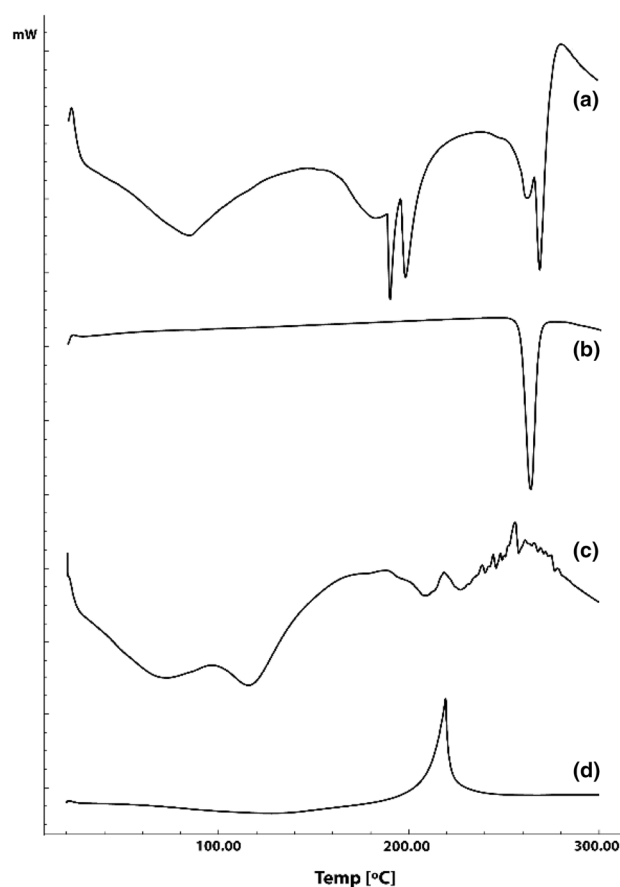

Fig. 7 DSC thermograms of (*a*) TEL, (*b*) SBE-β-CD, (*c*) physical mixture and (*d*) TEL-SBE-β-CD

endotherm at 88.9 °C ($\Delta H = -69.4$ J g^{-1}) and thermal degradation accompanied with solid state oxidation at 273.4 °C ($\Delta H = -42.13$ J g^{-1}). There were two small endotherms at around 193, and 210 °C which were not significant as ΔH was negligible. In the physical mixture, the melting peak of the drug shifted to 218.28 °C ($\Delta H = -8.8$ J g^{-1}) and that of SBE-β-CD to 236.8 °C ($\Delta H = -8.8$ J g^{-1}) with a drastic reduction in its intensity. The dehydration peak of SBE-β-CD also shifted from 88.9 °C to 78.7 °C ($\Delta H = -14.7$ J g^{-1}) to lower values with reduced intensity with an additional peak at 122.6 °C. ($\Delta H = -14.6$ J g^{-1}). The freeze-dried complex showed entirely a different spectrum compared to the physical mixture. Instead of endotherm, an exothermic appeared at 223 °C with the emission of heat ($\Delta H = +460.85$ J g^{-1}) indicating the formation of a new solid phase on entrapment of drug into the SBE-β-CD cavity [32]. Similar observations were reported in the case of amoxicillin [33].

FTIR spectra

FTIR spectrum of pure TEL showed the absorption bands at its major stretching vibrations corresponding

to the functional groups (Fig. 8) at 3063, 2957, 1695 and 1604 cm^{-1} representing the occurrence of aromatic C–H, aliphatic C–H of CH$_3$, a stretch of C=O in COOH and aromatic bending and stretching of C=C. Also, the characteristic peaks were seen in lower frequencies indicating the presence of aromatic C=C, C–O and aromatic bending of C–H at 1454, 1303 to 1236 and, 1012 and 750 cm^{-1} respectively. Prominent stretching vibrational peaks were seen in the FTIR spectrum of SBE-β-C at 3424, 2935, 1161, 1043, 1070 and 1043 cm^{-1} indicative of the presence of O–H, CH$_2$, O–H stretch of CH–OH, C–O stretch of CH$_2$OH, ether C–O–C and C–O of CH$_2$OH. It is has been well documented that the deviation observed in the absorption intensities in the FTIR spectra offers evidence related to the interaction of the functional groups within the samples tested [34].

The FTIR spectrum of the physical mixture was compared to its constituents. TEL showed no change in the position of the signal at 3063, 1263–1454 and 950–450 cm^{-1}
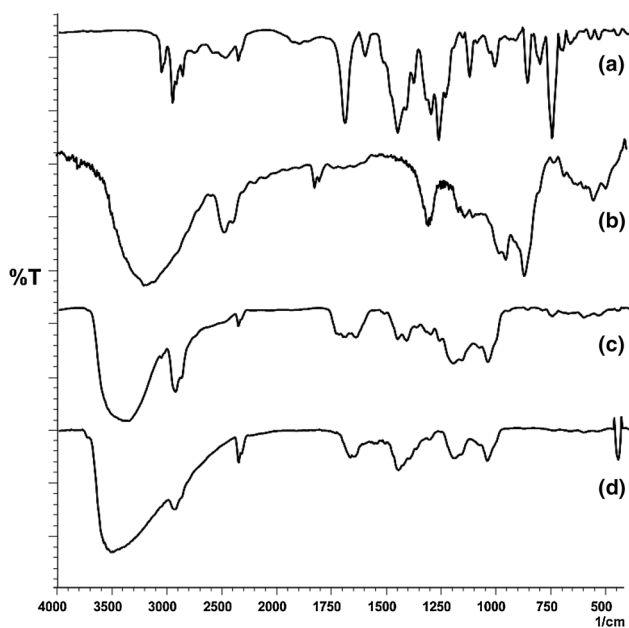

Fig. 8 FTIR spectra of (*a*) TEL, (*b*) SBE-β-CD, (*c*) physical mixture and (*d*) TEL-SBE-β-CD

with a slightly reduced intensity. But the signals which have shown a shift in cm^{-1} are 2957 to 2933, 1695 to 1701 (with a drastic reduction in the intensity), 1604 to 1645 and, 1012 to 1043 cm^{-1} (with minimized intensity). This indicates the involvement of the aliphatic side chain C=O, aromatic C=C and C–O–C side chain of TEL in the successful formation of the complex. Concerning the inclusion complex, SBE-β-CD, The signals at 1161 and 1043 cm^{-1} did not show any shift but the signal at 3424 cm^{-1} was largely shifted to 3356 cm^{-1}, and the signal at 2935 cm^{-1} disappeared. This indicated the involvement of the secondary –OH functional group of SBE-β-CD. From these observations, it could be summarized that there is slight interaction initiated in the solid state itself during grinding.

In the freeze-dried complex, the disappearance of drug signals was noticed at 3063, 2958, 1695 and 1600 cm^{-1}; in SBE- β-CD signals at 3424 and 1161 cm^{-1}. Shifting of the drug signals 2927 to 2939 cm^{-1} (C–H stretching), 1454 to 1448 cm^{-1} (C=O) and 1382–1398 cm^{-1} (C–O) of –COOH stretching. SBE-β-CD signals at 1653 to 1670 (C=O, H–O–H bending) indicate the involvement of side chain –COOH of TEL with primary –OH of SBE-β-CD with the formation of hydrogen bond in its interior [35, 36]. The exact –OH function interacting was further authenticated using NMR spectral data. However, FTIR spectra offered initial information about the functional group interaction of TEL within the cavity of SBE-β-CD.

P-XRD spectral analysis

The P-XRD patterns of pure TEL showed the presence (Fig. 9) of several sharp peaks indicative of its crystalline structure. The major peaks were found to be at a 2θ of ~6.52°, 13.91°, 14.80°, 18.10°, 18.71°, 19.23°, 22.15° and 24.81° with the corresponding intensities of 11309.93, 7752.45, 2164.13, 1392.74, 1836.11, 1217.56, 3086.37 and 1047.55. SBE-β-CD is an amorphous compound which was consistent with the PXRD pattern showing a blunt peak at 2θ of ~21.21° with an intensity of 2434. Upon complexation, the peaks of pure TEL was totally nullified with a retention of a blunt peak at ~20.13° and an intensity of 2314. The

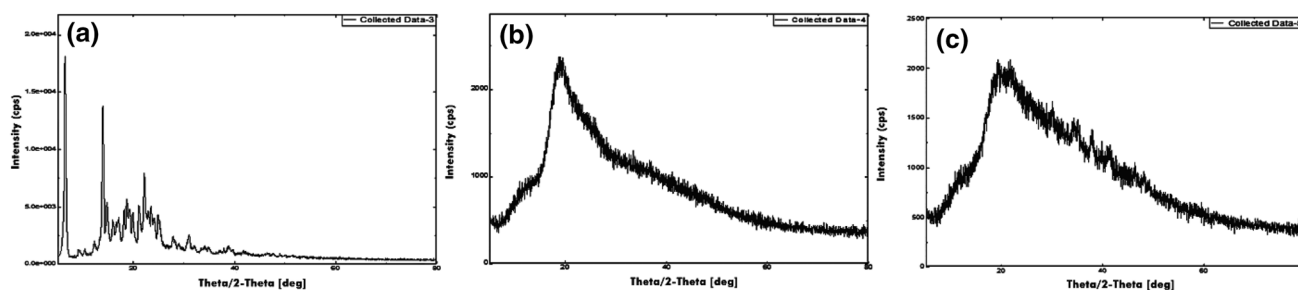**Fig. 9** P-XRD patterns of **a** TEL, **b** SBE-β-CD and **c** TEL–SBE-β-CD

results are in accordance with the fact that the XRD peaks of the guest molecule are non-superimposable with the complex after being incorporated into the guest molecule. The absence of the characteristic peaks is an indication of the conversion of the crystalline form to an amorphous form of the pure TEL after complexation with SBE-β-CD.

NMR spectral analysis

The ^{1}H-NMR spectrum of TEL, SBE-β-CD, and inclusion complex were analyzed (Fig. 10) and the majority of the signals of the complex were observed to be reduced in intensity demonstrating the restrictions provided by the guest molecule on inclusion. Intense interaction is taking place at the ring protons at H3 ($-\Delta\delta = 0.018$) and H6 ($-\Delta\delta = 0.008$) protons which are relatively more than the other protons of SBE-β-CD involving the side chain OH protons. As the H3 protons showed more upfield shift the most probable site could be H3 proton in the interior of the cavity. However, the exterior protruding proton at H6 is also partly involved which might have created a ring current in affecting the signal shift and the intensity. The steric hindrance due to the inclusion could also lead to these observations [37]. The signals corresponding to –CH$_2$ side chain is also reduced in intensity indicating the strain produced on the long aliphatic side chains. The side chain –OH signals showed considerable downfield shift indicating their involvement in the interaction (Table 2).

The shift in the NMR signal $\Delta\delta$ of the drug (not shown in the table) has shown a considerable downfield field shift. The signal at 12.86 corresponds to the aliphatic side chain COOH completely disappeared in the complex. This supports IR spectral data of the involvement of this functional group. All the aromatic protons showed a downfield shift to a $\Delta\delta = 0.3$–0.37. However, the signals corresponding to the protons of N–CH$_2$ at position 11 shown an upfield shift in δ from 5.629 to 5.102 ($-\Delta\delta = 0.527$) whereas the similar side chain at position 8 and 9 appearing at 2.928 and 1.828 were unaffected. This indicated that on inclusion, the N–CH$_2$–C

Table 2 Chemical shift (δ) and its variation (Δδ) SBE-β-CD in DMSO obtained from ^{1}H-NMR spectra

Protons assigned to SBE-β-CD	Pure SBE-β-CD	Freeze dried complex	±Δδ
H-1	4.957	4.959	+ 0.002
H-3	3.777/3.748	3.759 (intensified)	− 0.018
H-5	3.612	3.613	+ 0.001
H 6	3.56	3.552	− 0.008
H 2	3.348	3.344	− 0.004
H 4	3.347	3.343	− 0.004
CH$_2$ side chain	2.501	Reduced in intensity	–
CH$_3$ side chain	1.617	1.607	− 0.01
OH-side chain	4.47	4.854	+ 0.347
	4.41	4.707	+ 0.283

bond experienced a lot of strain restricting its vibrations. Probably at that point the drug is hanging out due to its giant size.

The ^{13}C-NMR signals of SBE-β-CD showed a shift (±Δδ) indicating an interaction between the guest and the host molecule when compared to the complex (Fig. 11). The signal at C2 showed considerable down-field shift compared to a little upfield shift in case of C5 and C6 (Table 3).

The signals corresponding to C1 and C4 were missing which may be due to restrictions offered by the guest to the host molecule. The missing signal at C3 could be due to strong coupling of the signals of the drug. A considerable upfield shift at the C2 site could be the site of interaction with the guest moiety. The C5 and C6 have also participated in the interaction. Concerning the drug TEL, many of the signals corresponding to aliphatic and ring carbons were found missing. However few of them have displayed an upfield shift of $\Delta\delta = + 0.03$. The signal corresponds to –COOH at far downfield 169.99 is seen to be missing in the spectra. The C11 carbon at N–CH$_2$–C– at $\delta = 46.6$ is also missing. The aliphatic side chains –CH$_2$ and –CH$_3$ at around 'δ' below 30 ppm shown a downfield shift of $\Delta\delta = 0.4$ to

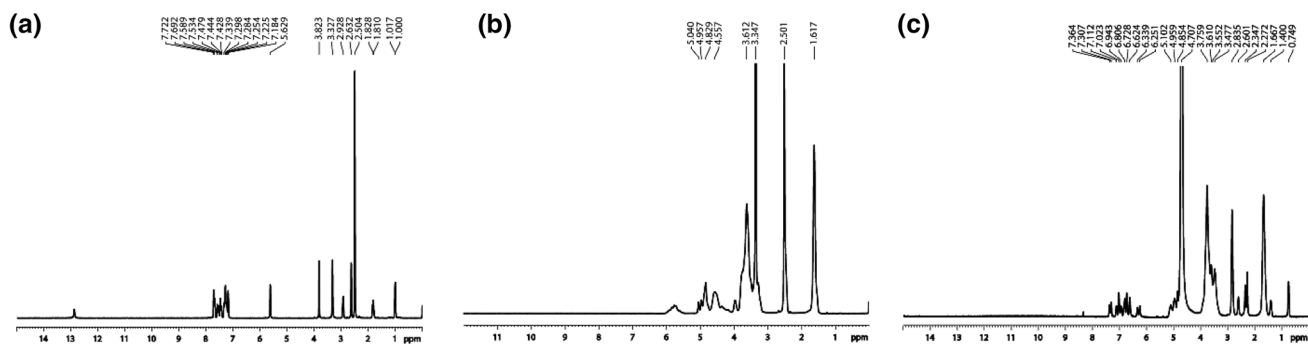**Fig. 10** ^{1}H-NMR spectra of **a** TEL, **b** SBE-β-CD and **c** TEL–SBE-β-CD
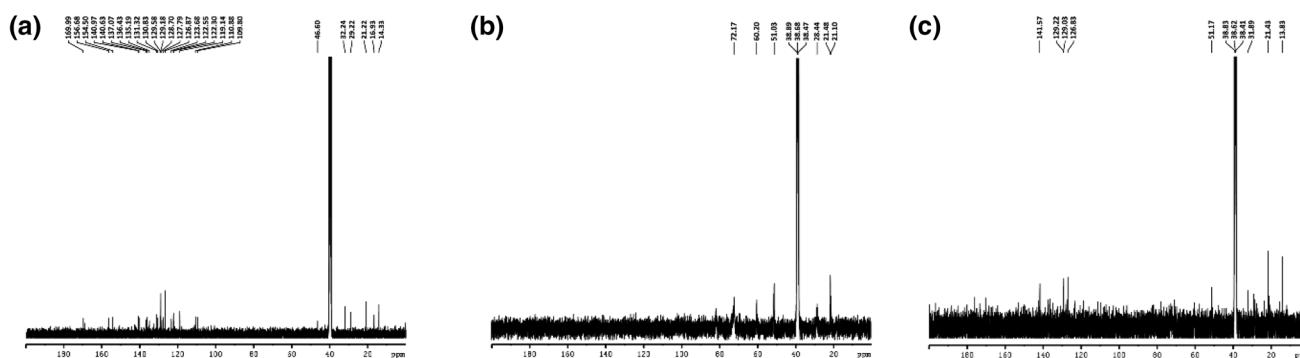
Fig. 11 ^{13}C-NMR spectra of **a** TEL, **b** SBE-β-CD and **c** TEL–SBE-β-CD

Table 3 ^{13}C-NMR spectral data of SBE-β-CD and the freeze-dried complex

Carbon assigned to SBE-β-CD	Pure SBE-β-CD	Freeze dried complex	± Δδ
C-1	72.17	Not traceable	
C-4	60.2	Not traceable	
C-2	51.03	51.17	+ 0.14
C-5	38.89–38.47	38.83–38.41	− 0.06
C-3	28.44	Not traceable	
C-6	21.48	21.43	− 0.05
Side chain	21.10	Not traceable	

0.7. These observations could lead to the conclusion that the C2 and C6 carbons at the exterior of the SBE-β-CD ring and C3 at the interior of the cavity at the wider rim, all have actively participated in the interaction with the drug. From the ^{1}H-NMR study, it was seen that even the H3 protons of SBE-β-CD are involved in the interaction indicated that part of the guest molecule entered from the wider end of the ring and the protons at the interior interact with the –COOH of the drug in the formation of hydrogen bond. The far end of the drug molecule is likely getting twisted around the C11 carbon moiety of N–CH$_2$–C, wraps around the guest molecule and then interacts with the protons at the exterior of it in C5 and C6 due to Vander Walls forces.

In vitro dissolution

The fate of the poorly soluble drugs exhibiting a pH-dependent dissolution behavior (like TEL) upon oral administration can be predicted by the dissolution tests carried out in biorelevant media. In all the three biorelevant media studied, the Tel-inclusion complex released 100% of TEL in 20 min whereas plain TEL released only 38% in FaSSGF (pH 1.6), 0.24% in FaSSIF (pH 6.5) and 0.15% in FeSSIF (pH 5).

In silico pharmacokinetic studies

Figure 12a showed the predicted and observed plasma concentration–time (PCT) profile after IV administration of TEL (10 mg). The simulated PCT profile was by the observed in vivo curve (data collected from literature) [27, 28] providing dependability of the disposition model in humans. On the other hand, the predicted plasma concentration–time
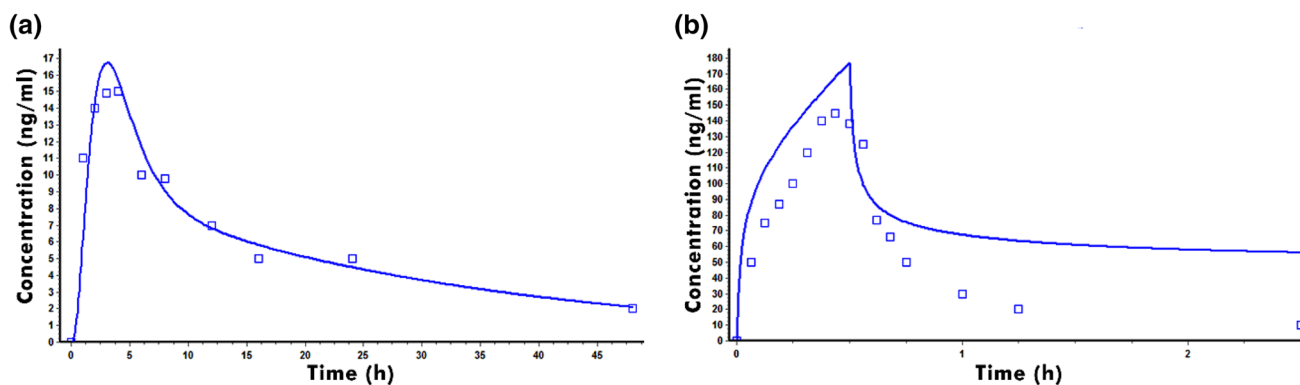

Fig. 12 a Observed (in square) and predicted (continuous line) plasma concentration–time profile following IV administration of TEL 10 mg; **b** observed (in square) and predicted (continuous line) plasma concentration–time curve following oral administration of 20 mg TEL

curve after oral administration of 20 mg TEL matched well with the observed curve (Fig. 12b), ascertaining the possibility of simulating the process of absorption. The observed and simulated parameters have been depicted in Table 4. Nearly superimposable profiles were obtained in the case of both the observed and simulated data. The fold error (FE) for the prediction accuracy of PK parameters was found to be < 2 signifying good prediction.

PK simulation for TEL inclusion complex in humans

The simulated PK parameters from plasma concentration–time profile for TEL inclusion complex after oral administration using the biorelevant dissolution profile is displayed in Table 4. The regional absorption profile is displayed in Fig. 13. GIT simulation of regional absorption shows that TEL is mainly absorbed through upper segments of intestine. There was very little amount absorbed from ileum (13% of total absorbed drug). The AUC_{0-t} and C_{max} values of TEL-inclusion complex were increased as compared to TEL tablet demonstrating enhanced oral absorption which may be due to increased TEL solubility.

Biorelevant dissolution aid simulation of in vivo conditions since they mimic physiological conditions in GIT. The GastroPlus™ software uses in silico-in vitro-in vivo approach. Successful prediction relies on the development of a robust absorption model built on valid assumptions and authentic inputs. Transporter-mediated processes require being taken into consideration for accurate predictions in humans as they are found to be accountable for clearance of permeability-limited compounds. Several in vitro assays measuring active processes have been developed, to enhance predictions for transporter substrates and PBPK models have been integrated with the active uptake rates assessed from these assays. OATP1B3 largely contributes to the hepatic uptake of TEL in human hepatocytes [27], and UDP-glucuronosyltransferase 1A3 is involved in metabolism [38, 39]. The enterohepatic recycling is a significant phase in the disposition of actively transported drugs and an essential process to include in an absorption model [40]. To take into account, the long half-life as a large volume of distribution observed in clinical data, deconjugation of glucuronide metabolite and enterohepatic recirculation of parent were therefore added to the absorption model. After building the absorption model that could describe ADME process of TEL in human, formulation factors were incorporated for prediction of formulation effect. Due to the increase in the solubility and thus exhibiting of an enhanced dissolution rate, the Tel inclusion complex presented higher bio absorption.

Table 4 Pharmacokinetic parameters of TEL IV, Oral and TEL-Inclusion complex administration obtained by in silico gastrointestinal compartmental simulation by GastroPlus™ software

Parameter	IV			Oral			TEL-inclusion complex
	Observed	Simulated	Fold error (FE)	Observed	Simulated	Fold error (FE)	
C_{max} (ng mL^{-1})	145	176.98	1.22	15	16.71	1.11	119
T_{max} (h)	0.43	0.5	1.14	4	3.1	0.775	3.94
AUC_{0-t} (ng h ml^{-1})	106.49	195.68	1.83	273	265.04	0.97	5001

Fig. 13 Regional absorption profile of TEL-inclusion complex from gastrointestinal tract
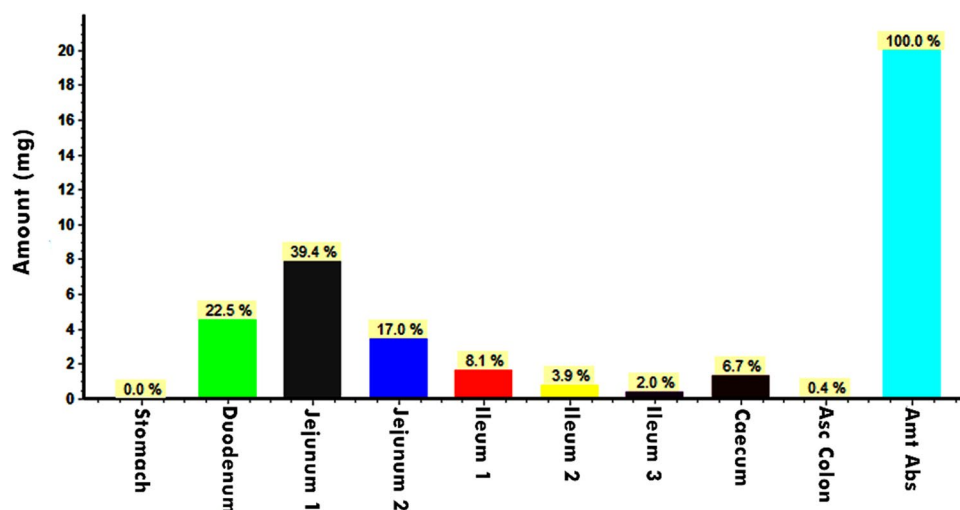
Conclusion

Results of the present study support the stable conformation of inclusion complex involving TEL and SBE-β-CD. Complexation resulted in a change in crystalline nature of TEL to amorphous. The predicted binding mode for TEL by the computational docking study with SBE-β-CD was in line with the experimental spectral recording for the inclusion complexes. The docking study predicted a tight fit binding of TEL within the cavity of SBE-β-CD by the involvement of hydrogen bonds and electrostatic interactions between them. Complexation enhanced solubility as well as dissolution rate of TEL. The simulated PCT profiles for IV and oral administration and the observed in vivo curve obtained from literature corresponded well with each other, proving the reliability of the absorption model. A good correlation between the in vitro tests and in silico modeling can be of great significance in improving our understanding and prediction of the in vivo behavior of various clinically relevant drugs and their products.

References

1. Wienen, W., Entzeroth, M., Meel, J.C.A., Stangier, J., Busch, U., Ebner, T., Schmid, J., Lehmann, H., Matzek, K., Kempthorne-Rawson, J., Gladigau, V., Hauel, H.N.: A review on telmisartan: a novel, long-acting angiotensin II-receptor antagonist. Cardiovasc. Drug. Rev. **18**, 127–154 (2006)
2. Kaur, M., Bhatia, R.K., Pissurlenkar, R.R.S., Coutinho, E.C., Jain, U.K., Katare, O.P., Chandra, R., Madan, J.: Telmisartan complex augments solubility, dissolution and drug delivery in prostate cancer cells. Carbohydr. Polym. **101**, 614–622 (2014)
3. Abali, H., Güllü, I.H., Engin, H., Haznedaroğlu, I.C., Erman, M., Tekuzman, G.: Old antihypertensives as novel antineoplastics: angiotensin-I-converting enzyme inhibitors and angiotensin II type 1 receptor antagonists. Med. Hypotheses **59**, 344–348 (2002)
4. Sharpe, M., Jarvis, B., Goa, K.L.: Telmisartan: a review of its use in hypertension. Drugs **61**(10), 1501–1529 (2001)
5. McClellan, K.J., Markham, A.: Telmisartan. Drugs **56**(6), 1039–1044 (1998)
6. Park, J., Park, H.J., Cho, W., Cha, K.-H., Yeon, W., Kim, M.S., Kim, J.S., Hwang, S.: Comparative study of telmisartan tablets prepared via the wet granulation method and prior? Prepared using the spray-drying method. J. Arch. Pharm. Res. **34**, 463–468 (2011)
7. Tran, P.H.L., Tran, H.T.T., Lee, B.J.: Modulation of microenvironmental pH and crystallinity of ionizable telmisartan using alkalizers in solid dispersions for controlled release. J. Control. Rel. **129**, 59–65 (2008)
8. Sangwai, M., Vavia, P.: Amorphous ternary cyclodextrin nanocomposites of telmisartan for oral drug delivery: improved solubility and reduced pharmacokinetic variability. Int. J. Pharm. **453**, 423–432 (2013)
9. Van Hoogevest, P., Liu, X., Fahr, A.: Drug delivery strategies for poorly water-soluble drugs: the industrial perspective Expert Opin. Drug Deliv. **8**(11), 1481–1500 (2011)
10. Singh, A., Worku., Z.A., Van den Mooter, G.: Oral formulation strategies to improve solubility of poorly water-soluble drugs. Expert Opin. Drug Deliv. **8**(10), 1361–1378 (2011)
11. Davis, M.E., Brewster, M.E.: Cyclodextrin-based pharmaceutics: past, present and future. Nat. Rev. Drug Discov. **3**, 1023–1035 (2004)
12. Zia, V., Rajewski, R.A., Stella, V.: Effect of cyclodextrin charge on complexation of neutral and charged substrates: comparison of (SBE)7M-beta-CD to HP-beta-CD. J. Pharm. Res. **18**, 667–673 (2001)
13. Irie, T., Uekama, K.: Pharmaceutical applications of cyclodextrins: III: toxicological issues and safety evaluation. J. Pharm. Sci. **86**, 147–162 (1997)
14. Thompson, D.O.: Cyclodextrins-enabling excipients: their present and future use in pharmaceuticals. Crit. Rev. Ther. Drug Carrier Syst. **14**, 1–104 (1997)
15. Dinnebier, R.E., Sieger, P., Nar, H., Shankland, K., David, W.I.F.: Structure characterization of three crystalline modifications of telmisartan by single crystal and high-resolution X-ray powder diffraction. J. Pharm. Sci. **89**, 1465–1479 (2000)
16. Wang, J., Pham, D., Kee, T.W., Clafton, S.N., Guo, X., Clements, P., Lincoln, S.F., Prud'homme, R.K., Easton, C.J.: Aggregation and host–guest interactions in dansyl-substituted poly(acrylate)s in the presence of β-cyclodextrin and a β-cyclodextrin dimer in aqueous solution: a UV-Vis, fluorescence, 1H NMR, and rheological study. Macromolecules **44**, 9782–9791 (2011)
17. Kiwon, O.K., Jung, Y.W., Jee, J., Byun, Y.: Facile docking and scoring studies of carborane ligands with estrogen receptor. Bull. Korean Chem. Soc. **34**, 1051–1054 (2013)
18. Galek, P.T.A., Fabian, L., Allen, F.H.: Universal prediction of intramolecular hydrogen bonds in organic crystals. Acta Crystallogr. B 66, 237–252 (2010)
19. Wood, P.A., Feeder, N., Furlow, M., Galek, P.T.A., Groom, C.R., Pidcock, E.: Knowledge-based approaches to co-crystal design. CrystEngComm 16, 5839–5848 (2014)
20. Martiny, V.Y., Martz, F., Selwa, E., Iorga, B.I.: Blind pose prediction, scoring, and affinity ranking of the CSAR 2014 dataset. J. Chem. Inf. Model. S6, 996–1003 (2016)
21. Higuchi, T., Connors, K.A.: Phase solubility techniques. Adv. Anal. Chem. Instrum. **4**, 117–212 (1965)
22. Williams, R.O., Mahaguna, V., Sriwongjanya, M.: Characterization of an inclusion complex of cholesterol and hydroxypropyl-beta-cyclodextrin. Eur. J. Pharm. Biopharm. **46**, 355–360 (1998)
23. Klein, S.: The use of biorelevant dissolution media to forecast the in vivo performance of a drug. AAPS J. **12**, 397–406 (2010)
24. Zoeller, T., Dressman, J.B., Klein, S.: Application of a ternary HP-β-CD-complex approach to improve the dissolution performance of a poorly soluble weak acid under biorelevant conditions. Int. J. Pharm. **430**, 176–183 (2012)
25. Fagerberg, J.H., Tsinman, O., Sun, N., Tsinman, K., Avdeef, A., Bergstrom, C.A.S.: Dissolution rate and apparent solubility of poorly soluble drugs in biorelevant dissolution media. Mol. Pharm. **7**, 1419–1430 (2010)
26. George, J.K., Singh, S.K., Verma, P.R.P.: In vivo in silico pharmacokinetic simulation studies of carvedilol-loaded nanocapsules using GastroPlus. Ther. Deliv. **7**, 305–318 (2016)
27. Ishiguro, N., Maeda, K., Kishimoto, W., Saito, A., Harada, A., Ebner, T., Roth, W., Igarashi, T., Sugiyama, Y.: Predominant contribution of OATP1b3 to the hepatic uptake of telmisartan, an angiotensin ii receptor antagonist, in humans. Drug Metab. Dispos. **34**, 1109–1115 (2006)
28. Stangier, J., Schmid, J., Türck, D., Switek, H., Verhagen, A., Peeters, P.A., van Marle, S.P., Tamminga, W.J., Sollie, F.A., Jonkman, J.H.: Absorption, metabolism, and excretion of intravenously

and orally administered [14C] telmisartan in healthy volunteers. J. Clin. Pharmacol. **40**, 1312–1322 (2000)

29. Li, R., Barton, H.A., Maurer.:, T.S.: A Mechanistic Pharmacokinetic model for liver transporter substrates under liver cirrhosis conditions. CPT **4**, 338–349 (2015)

30. Stangier, J., Su, C.P.F., Schöndorfer, G., Roth, W.: Pharmacokinetics and safety of intravenous and oral telmisartan 20 mg and 120 mg in subjects with hepatic impairment compared with healthy volunteers. J. Clin. Pharmacol. **40**, 1355–1364 (2000)

31. De Buck, S.S., Sinha, V.K., Fenu, L.A., Nijsen, M.J., Mackie, C.E., Gilissen, R.A.H.J.: Prediction of human pharmacokinetics using physiologically based modeling: a retrospective analysis of 26 clinically tested drugs. Drug Metab. Dispos. **35**, 1766–1780 (2007)

32. Grandelli, H.E., Stickle, B., Whittington, A., Kiran, E.: Inclusion complex formation of β-cyclodextrin and naproxen: a study on exothermic complex formation by differential scanning calorimetry. J. Incl. Phenom. Macrocycl. Chem. **77**, 269–277 (2013)

33. Bisson-Boutelliez, C., Fontanay, S., Finance, C., Kedzierewicz, F.: Preparation and physicochemical characterization of amoxicillin beta-cyclodextrin complexes. AAPS PharmSciTech **11**, 574–581 (2010)

34. Ge, X., Huang, Z., Tian, S., Huang, Y., Zeng, C.: Complexation of carbendazim with hydroxypropyl-β-cyclodextrin to improve solubility and fungicidal activity. Carbohydr. Polym. **89**, 208–212 (2012)

35. Zhang, Y., Zhi, Z., Jiang, T., Zhang, J., Wang, Z., Wang, S.: Spherical mesoporous silica nanoparticles for loading and release of the poorly water-soluble drug telmisartan. J. Control. Release **145**, 257–263 (2010)

36. Chella, N., Narra, N., Rama Rao, T.: Preparation and characterization of liquisolid compacts for improved dissolution of telmisartan. J. Drug Deliv. **2014**, 692793 (2014)

37. Zhao, R., Tan, T., Sandstrorm, C.: NMR studies on puerarin and its interaction with beta-cyclodextrin. J. Biol. Phys. **37**, 387–400 (2011)

38. Ieiri, I., Nishimura, C., Maeda, K., Sasaki, T., Kimura, M., Chiyoda, T., Hirota, T., Irie, S., Shimizu, H., Noguchi, T., Yoshida, K., Sugiyama, Y.: Pharmacokinetic and pharmacogenomic profiles of telmisartan after the oral microdose and therapeutic dose. Pharmacogenet. Genom. **21**, 495–505 (2011)

39. Yamada, A., Maeda, K., Ishiguro, N., Tsuda, Y., Igarashi, T., Ebner, T., Roth, W., Ikushiro, S., Sugiyama, Y.: The impact of pharmacogenetics of metabolic enzymes and transporters on the pharmacokinetics of telmisartan in healthy volunteers. Pharmacogenet. Genom. **21**, 523–530 (2011)

40. Fagerholm, U.: Prediction of human pharmacokinetics-biliary and intestinal clearance and enterohepatic circulation. J. Pharm. Pharmacol. **60**, 535–542 (2008)